The Sensitivity of the Arctic Ocean Sea Ice Thickness and Its Dependence on the Surface Albedo Parameterization

GÖRAN BJÖRK AND CHRISTIAN STRANNE

Department of Earth Sciences, University of Gothenburg, Gothenburg, Sweden

KARIN BORENÄS

SMHI, Västra Frölunda, Sweden

(Manuscript received 6 February 2012, in final form 6 August 2012)

ABSTRACT

In this study, the response of sea ice thickness to changes in the external forcing is investigated and particularly how this response depends on the surface albedo formulation by means of a one-dimensional coupled ocean–ice–atmosphere model. The main focus is on the thickness response to the atmospheric heat advection F_{wall}, solar radiation F_{SW}, and amount of snow precipitation S_{prec}. Different albedo parameterization schemes [ECHAM5, CSIRO, and Community Climate System Model, version 3 (CCSM3)] representing albedos commonly used in global climate models are compared together with more simplified schemes. Using different albedo schemes with the same external forcing produces large differences in ice thickness. The ice thickness response is similar for all realistic albedo schemes with a nearly linear decrease with increasing F_{wall} in the perennial ice regime and with a steplike transition into seasonal ice when F_{wall} exceeds a certain threshold. This transition occurs at an annual-mean ice thickness of 1.7–2.0 m. Latitudinal differences in solar insolation generally leads to increasing ice thickness toward the North Pole. The snow response varies significantly depending on which albedo scheme is used. The ECHAM5 scheme yields thinner ice with S_{prec}, the CSIRO scheme gives ice thickness nearly independent of S_{prec}, and with the CCSM3 scheme the ice thickness decreases with S_{prec}. A general result is that the modeled ice cover is rather sensitive to positive perturbations of the external heat supply when it is close to the transition such that just a small increase of, for example, F_{wall} can force the ice cover into the seasonal regime.

1. Introduction

The Arctic pack ice has been reduced during the last decades, in terms of both area extent and volume. The ice extent at the summer minimum in September has shown a negative trend of around 11% per decade for the period 1979–2007 relative to the 1979 value (Perovich and Richter-Menge 2009) based on satellite data, and the mean ice thickness has been reduced from 3.4 m in 1980 to about 2.3 m in 2000 according to submarine data (Rothrock et al. 2008). Accompanying the overall ice reduction there has also been a considerable change of ice types with a loss of up to 40% of thick and old multiyear ice (Maslanik et al. 2007; Kwok et al. 2009). The minimum summer ice extent had a record low in 2007 and again in 2011 at about 60% of the long-term average (1979–2000) (e.g., Comiso et al. 2008).

The mechanisms driving the observed sea ice decline are the subject of considerable research (e.g., Serreze et al. 2007b; Kwok 2011). The principal tool for projections are global climate models (GCMs) that simulate conditions for the twentieth century and projections for the twenty-first century based on a range of CO_2 emission scenarios. These models show a large intermodel scatter of the Arctic Ocean ice thickness, basinwide ice distribution, and areal extent in the twentieth-century simulations (e.g., Holland et al. 2010). Scenario runs into the twenty-first century show generally a thinning, but again with a considerable intermodel scatter (Holland et al. 2010). Another tool is to use regional climate models (RCMs) run under prescribed boundary forcing obtained from GCMs. A similar intermodel scatter is also found for the regional Arctic climate models (Rinke

Corresponding author address: Göran Björk, Department of Earth Sciences, University of Gothenburg, Box 460, SE-40530 Gothenburg, Sweden.
E-mail: gobj@gvc.gu.se

DOI: 10.1175/JCLI-D-12-00085.1

et al. 2006; Wyser et al. 2008). Analyses of the reason behind the intermodel scatter for both GCMs and RCMs point at the surface albedo parameterization as one of the major factors and at the importance of a correct representation of the albedo feedback mechanism (Holland et al. 2010; Wyser et al. 2008). The importance of the surface albedo for the ice thickness has further been shown in stand-alone basin-scale dynamic–thermodynamic two-dimensional (2D) ice models (Liu et al. 2007), in single column models (Holland and Curry 1999), and in more idealized model concepts (e.g., Eisenman and Wettlaufer 2009).

The variation in snow/ice albedo is one of the most important factors influencing the Arctic energy budget and the stability of the Arctic sea ice (e.g., Curry et al. 1995; Houghton et al. 2001). The surface albedo is, however, a rather complex quantity that is reflected by the many existing types of parameterizations used in models. It is a function of surface characteristics including snow depth, ice thickness, snow crystal structure, and melt ponds (area fraction and depth). It is also dependent on solar zenith angle and on the atmospheric properties.

Since the overall Arctic climate system is highly complex, there is a need to make idealized studies of specific parts of the system in order to gain a better understanding. One type of idealization is to use a coupled atmosphere–ice–ocean column model. The basic concept is relatively simple, although various types of column models with different degree of complexity have been developed (e.g., Thorndike 1992; Holland and Curry 1999; Björk and Söderkvist 2002). In this kind of models the Arctic atmosphere, ice cover and ocean are represented by one single vertical column. Energy reaches the polar column from the sun and through net supply of energy from lower latitudes carried by the atmospheric and oceanic circulation. The system loses energy through infrared radiation back to space. Depending on the energy supply, the Arctic Ocean will respond by forming either a perennial ice cover of a certain average thickness, a seasonal ice cover, or a completely ice-free ocean. A benefit of coupled atmosphere–ice–ocean column models is that the model forcing can be prescribed at the vertical boundaries of the model instead of at the ocean surface. The coupled column approach then gives the ice cover more freedom to evolve according to the external forcing than for prescribed surface forcing. For example, a prescribed atmospheric near-surface temperature constrains the melt season to start when the temperature reaches 0°C early in the summer, while in a coupled model the start of the melt season becomes a function of the atmospheric properties, the surface albedo, the latitude, the amount of precipitation, and the heat supply through atmospheric and oceanic advection. A further advantage of a column model is that it is possible to cover a large and relatively dense range in the forcing parameter space. A disadvantage is that horizontal variations within the Arctic Ocean of quantities like the ice thickness are not resolved.

Another type of idealization is to exclude some feedback mechanisms in order to obtain a more direct response to changes in model quantities of special interest. For example, in a fully coupled system including all feedbacks a change in the albedo will affect the cloudiness and then the precipitation that in turn will change the albedo (which is dependent on the amount of snow). Such feedback chains makes it hard to evaluate the effect of the albedo parameterization alone since the net effect on the system will be dependent on the, often uncertain, parameterizations of the separate links.

In this study we investigate the response of sea ice thickness to changes in the external forcing and, particularly, how this response depends on the surface albedo formulation. We have no intention to find the best possible albedo scheme but rather to show in a controlled way how the albedo scheme will influence the response of the Arctic Ocean sea ice cover. This is done by means of a Coupled Column Arctic Model (CCAM) in which we vary one of the external forcing parameters while keeping all other types of forcing at fixed values (or fixed annual cycles). The advantage of this type of experiments is that a particular single process (in this case the albedo feedback) can be isolated and studied under controlled but variable external conditions. This is in contrast to fully coupled global models in which different albedo schemes will not only have a local effect on the ice cover but also affect other critical quantities such as the atmospheric circulation and cloudiness that then feeds back on the sea ice properties. The direct effect of the albedo parameterization might also be hidden behind the noise of large natural model variability.

As previously mentioned, a typical feature of the column model approach is that fluxes of various quantities across the model border (boundary fluxes) have to be specified. These fluxes serve also as natural forcing parameters. Here we focus on the Arctic Ocean sea ice thickness and its response to two types of boundary fluxes: the meridional atmospheric energy advection F_{wall} and the solar insolation at the top of the atmosphere F_{SW}. The boundary flux F_{wall} describes the amount of energy that is carried, mainly by warm air masses, northward across 70°N. The atmospheric energy advection and solar incidence are two of the three dominating parts of the Arctic heat budget. The

atmospheric energy advection corresponds to roughly 100 W m^{-2} (annual average) and the insolation at the top of the atmosphere to about 180 W m^{-2} (annual average) in the contemporary climate regime (Thorndike 1992). The third dominating part is the infrared radiation back to space, which is computed as an internal quantity in the model and thus does not have to be specified. The oceanic heat flux is much smaller, 1–6 W m^{-2}, depending on the type of estimate and location, but can still have a significant impact on the ice thickness (Polyakov et al. 2010). Variations of the oceanic boundary conditions are not treated specifically in this study.

Finally we also examine the effect of changing the amount of snow precipitation. This parameter is natural to have as a prescribed and variable quantity in this type of study since it is largely an unknown quantity, which is difficult to model owing to its strong interaction with the surface albedo and the not-well-understood cloud and water vapor dynamics of the Arctic atmosphere (e.g., Verlinde et al. 2007; Soden and Held 2006). Model-generated snow precipitation is also difficult to validate because of the scarce precipitation data available for the central Arctic.

2. Method

a. Model description

The model used in the study is a fully coupled ocean–ice–atmosphere column model. The ocean model (Björk 1989) can be seen as a sophisticated lower boundary condition for the ice model controlling the freshwater content in the system and the upper-ocean dynamics. It includes detailed upper-ocean dynamics with mixed layer deepening due to mechanical mixing and negative buoyancy flux during winter. The mixed layer retreats during summer due to ice melting and positive buoyancy flux. The ocean model handles supply of freshwater from rivers, inflow from Bering Strait, and a geostrophic outflow. The areal ice export is prescribed but is actively incorporated in the freshwater balance. The model ice cover is separated into 40 ice categories, each evolving independently according to the thermodynamic forcing (Björk 1997). The thermodynamic module for each category has one internal temperature point in the ice and allows for internal heating due to penetrating solar radiation. The effect of salt in brine pockets is also included. It should be noted that there exist more sophisticated ice models with several more internal temperature points both in ice and snow (e.g., Cheng et al. 2008), but we judge that our model represents a fair trade-off between complexity and computational cost for the present purpose, including multiple runs to steady state over a wide and dense multidimensional parameter space.

The atmospheric part of the model is a standalone version of the column radiation code employed by the National Center for Atmospheric Research Community Climate Model version 3 (CCSM3) (Collins et al. 2006). It has a vertical grid of 18 layers. A convective adjustment scheme and an internal heat source in each layer, corresponding to the external energy supply at the vertical boundary (F_{wall}), are added in the present application. The sea ice model is coupled with the ocean and atmosphere models so that the heat and salt fluxes passed on to the ocean component and the surface temperature and turbulent and radiative heat fluxes passed on to the atmospheric component are based on weighted averages over all ice categories (including open water).

To generate a realistic ice cover with a thickness distribution including an open water fraction it is necessary to introduce some sort of ice deformation process. Here the deformation is described by areal ice export, representing divergent motions and an associated loss of ice volume from the model domain, and ridging, which is represented by thin ice piled up into thicker ice (but not affecting the total ice volume per se). The ice export is controlled by a parameter D representing ice divergence rate. For the basin as a whole D is related to the areal ice export as $D = A_{\text{ex}}/A_B$, where A_{ex} is the areal export and A_B the area of the Arctic Ocean ($A_B = 0.78 \times 10^{13}$ m^2). The degree of ridging is basically controlled by one parameter r, the amount of open water formed by the ridging process each year. In the present model runs $r = 0.4$ yr^{-1}; that is, an open water area corresponding to 40% of the basin area is formed each year by the ridging process. Note that the actual open water area in the model is much smaller than 40% since newly formed open water freezes over rapidly during winter. The ridging is turned off when the open water fraction raises above a certain value (5%) during summer. Other properties of the ridging process are governed by a participation parameter, controlling which part of the thinnest fraction of the ice cover participates in the ridging, and a thickness multiplier [for a complete description, see Björk (1997)]. The divergence has a similar effect as r by forming open water at the rate D while the same area fraction is removed from each ice category, thus reducing the total ice volume. The value of D follows a prescribed annual cycle in the model based on the export in Fram Strait (see Table 1). The average ice thickness is defined as

TABLE 1. Model forcing and seasonal-dependent parameters (for additional parameters, see Björk and Söderkvist 2002). The parameter α_{snow} is the annual cycle of snow albedo in the Maykut surface albedo parameterization; CWP: cloud water path and CF: cloud fraction.

	Jan	Feb	Mar	Apr	May	Jun	Jul	Aug	Sep	Oct	Nov	Dec
F_{wall} (W m^{-2})	118.3	108.5	107.5	92.6	72.6	72.8	72.6	78.3	98.1	97.3	112.3	108.4
D (10^{-9} s^{-1})	5.4	5.4	5.3	5.1	3.0	4.3	3.8	3.7	4.3	4.3	5.0	5.7
CF_{high}	0.08	0.09	0.06	0.02	0.01	0.02	0.04	0.04	0.04	0.04	0.05	0.07
CF_{mid}	0.50	0.50	0.49	0.34	0.22	0.25	0.29	0.32	0.34	0.37	0.44	0.49
CF_{low}	0.11	0.10	0.11	0.17	0.20	0.20	0.20	0.20	0.21	0.23	0.16	0.12
CWP_{high} (g m^{-2})	5	5	5	5	20	30	30	30	30	10	5	5
CWP_{mid} (g m^{-2})	12	12	12	12	12	12	12	12	12	12	12	12
CWP_{low} (g m^{-2})	8	8	8	8	8	8	8	8	8	8	8	8
α_{snow}	0.85	0.84	0.83	0.81	0.82	0.78	0.64	0.69	0.84	0.85	0.85	0.85
S_{prec} (mm day^{-1})	1	0.9	0.9	0.7	0.7	0.9	1.4	1.6	1.6	1.4	1.1	1.0

$$h_{ice} = \overline{h'_{ice}} = \overline{\sum_{i=1}^{N} a_i H_i},$$

where h_{ice} is the annual mean of the distribution mean thickness h'_{ice}. The overbar denotes an annual-mean operator, a_i is the area fraction of ice category i, H_i the thickness of category i, and N the total number of categories in the model. The model has been shown to generate a realistic annual-mean ice thickness distribution and realistic seasonal cycles of melting, freezing, open water fraction, near-surface air temperature, oceanic heat flux, and ocean stratification when run under 1990s external forcing conditions (Björk and Söderkvist 2002).

b. Model forcing and prescribed internal quantities

The most relevant forcing parameters and prescribed internal quantities are presented below and summarized in Table 1. For additional parameters the reader is referred to Björk and Söderkvist (2002).

The baseline F_{wall} follows a climatological cycle calculated from the National Centers for Environmental Prediction (NCEP) reanalysis data from 1954 to 2001 using the algorithm presented by Overland and Turet (1994). The net divergence D (which is related to the areal ice export) follows a fixed seasonal cycle taken from Kwok and Rothrock (1999). Climatological precipitation is calculated from the *Arctic Meteorology and Climate Atlas* (Arctic Climatology Project 2000), where only area-weighted ocean grid cells have been considered.

The climatological precipitation in snow equivalent, S_{prec}, was trimmed by a factor 1.5 so that the maximum snow depth equals 0.3 m. Clouds occupy a certain fraction (CF) of the sky at three different levels and follow an annual climatological cycle calculated from the International Satellite Cloud Climatology Project (ISCCP) D2 dataset (Rossow and Duenas 2004). Each cloud layer has a specified cloud water path (CWP) that follows an annual climatological cycle according to Björk and Söderkvist (2002). It should be noted that the cloud data during the polar night are difficult to validate and that the error in these might be large. Atmospheric water vapor is prescribed and follows an annual climatological cycle calculated for each month and pressure level from the NCEP–NCAR reanalysis data (not shown).

c. Albedo parameterizations

We start with the simplest possible albedo formulation, a constant albedo (=0.65), equal for all surface types no matter if it is ice, snow, or open water. Then we introduce a more realistic albedo formulation with a seasonal-dependent snow albedo and thickness-dependent ice albedo, where zero thickness represents open water. The remaining three albedo types are parameterizations used in climate model simulations and are chosen from 25 models that were participating in the CMIP3 model intercomparison project (Meehl et al. 2007). Almost all models in the CMIP3 project have, in fact, different types of albedo schemes although the differences are sometimes small. The various albedo schemes can be assigned to four major groups: 1) temperature dependence using a step function [represented by, e.g., Commonwealth Scientific and Industrial Research Organisation Mark version 3.0 (CSIRO Mk3) and the Meteorological Institute of the University of Bonn (MIUB) ECHAM and the global Hamburg Ocean Primitive Equation (ECHO-G)]; 2) temperature dependence using a ramp function between a temperature significantly below freezing and the melting point [the third climate configuration of the Met Office Unified Model (HadCM3); Model for Interdisciplinary

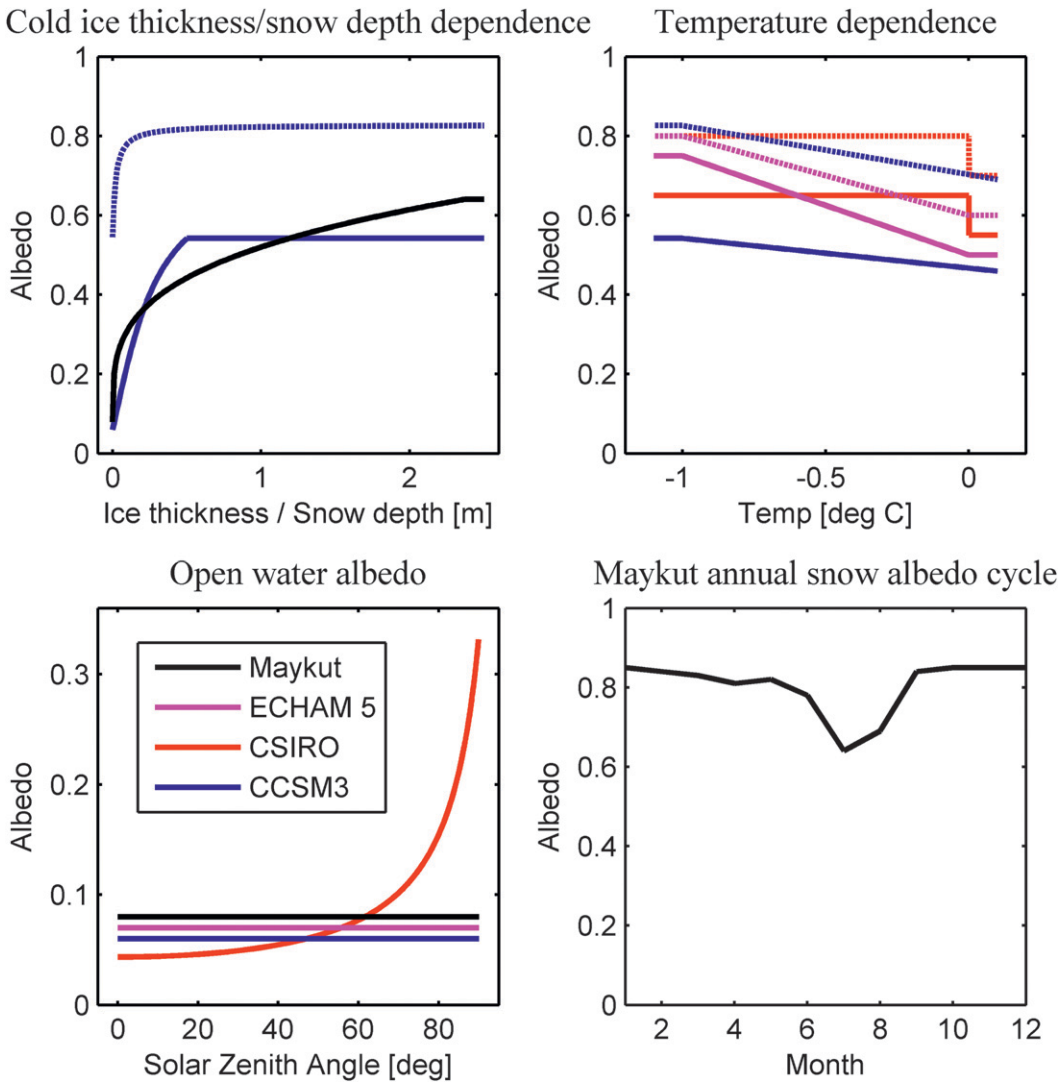

FIG. 1. Basic properties of the albedo parameterizations used in the study. Solid lines represent ice albedo, and dashed lines snow albedo.

Research on Climate 3.2, medium-resolution version (MIROC3.2medres); and ECHAM5]; and 3) albedo dependent on surface temperature, snow thickness, and ice thickness [Community Climate System Model, version 3 (CCSM3) and Bjerknes Centre for Climate Research (BCCR)]. A fourth group would be snow albedo based on snow age [Centre National de Recherches Météorologiques (CNRM)], which we cannot test here since the present model does not include this variable. We have chosen CSIRO Mk3, ECHAM5, and CCSM3 to represent each group. CCSM3 applies the most sophisticated albedo scheme, which is also dependent on wavelength bands. The basic characteristics of the chosen albedo schemes are shown in Fig. 1, and a detailed description is given in the appendix.

The albedo is calculated separately for each thickness category but is passed on to the atmosphere as a weighted average over the ice thickness categories. For CCSM3 the albedo is kept separated in the spectral bands when passed on to the atmosphere, while the ice model uses a weighted average over the spectrum.

3. Results

The model is run over 50 years with a time step of 2 h using monthly climatological forcing until it reaches a steady state during the last part of the simulation with nearly identical repetitive annual cycles of the prognostic variables, such as the ice thickness. Repeating this procedure over a range of external forcing values results

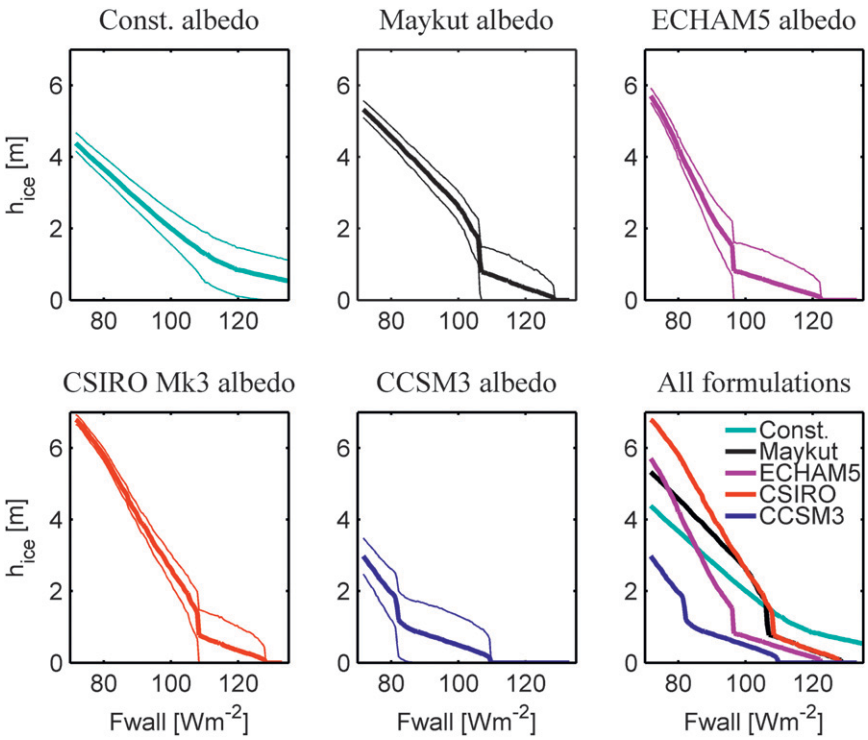

FIG. 2. Response curves for different albedo parameterizations at latitude 80°N. Thick lines show the annual-mean ice thickness h_{ice}. Upper (lower) thin lines show annual maximum (minimum) ice thickness. Boundary flux F_{wall} is the meridional atmospheric energy advection.

in response curves showing how model quantities such as the annual-mean ice thickness depends on the external forcing. We then change the albedo parameterization and compute a new response curve.

a. Response to changes in F_{wall}

Figure 2 shows the ice thickness dependence on the annual mean F_{wall} for the different albedo formulations. The upper and lower thin curves show the maximum and minimum ice thickness over the year. The ice cover is thus in a seasonal regime when the lower curve is at zero. A constant albedo (Fig. 2a) gives a linear response for low values of F_{wall} and a relatively smooth transition into seasonal ice, which occurs for a value ~120 W m^{-2}. The slope of the response curve is equivalent to the sensitivity of the ice thickness to changes in the forcing, and the sensitivity is therefore significantly smaller in the seasonal regime compared to the regime with perennial ice.

All other more realistic albedo schemes have in common that, instead of a smooth response curve, there is a steplike transition into a seasonal regime with a substantial reduction of the ice thickness when F_{wall} is increased beyond a threshold value. This is basically a result of the large albedo contrast between ice and open water (discussed in more detail below). Although the basic shape of the response curves is similar for all nonconstant albedo schemes, there are important differences. The transition into the seasonal regime occurs for an annual mean F_{wall} of ~107 W m^{-2} for Maykut and CSIRO while it occurs at 96 W m^{-2} for ECHAM5 and as low as 82 W m^{-2} for CCSM3. As the typical value of F_{wall} based on atmospheric data is about 100 W m^{-2} (Serreze et al. 2007a) this means that the two latter albedo schemes are not able to maintain a perennial ice cover in this model setup. The value for which the ocean becomes completely ice free varies also between the albedo schemes but to a lesser degree than for the transition between seasonal and perennial ice. Comparing the slopes of the curves (Fig. 2f), it is clear that both ECHAM5 and CSIRO schemes produce steeper slopes in the perennial regime, meaning that these albedo schemes yield larger sensitivity of the ice thickness to changes in the atmospheric heat transport compared to the Maykut and CCSM3 schemes.

The CCSM3 albedo scheme stands out by causing much thinner ice than the other albedo schemes. This is due to the generally darker CCSM3 albedo parameterization, including the lowest bare ice albedo of all formulations and a rather low snow albedo due to the snow

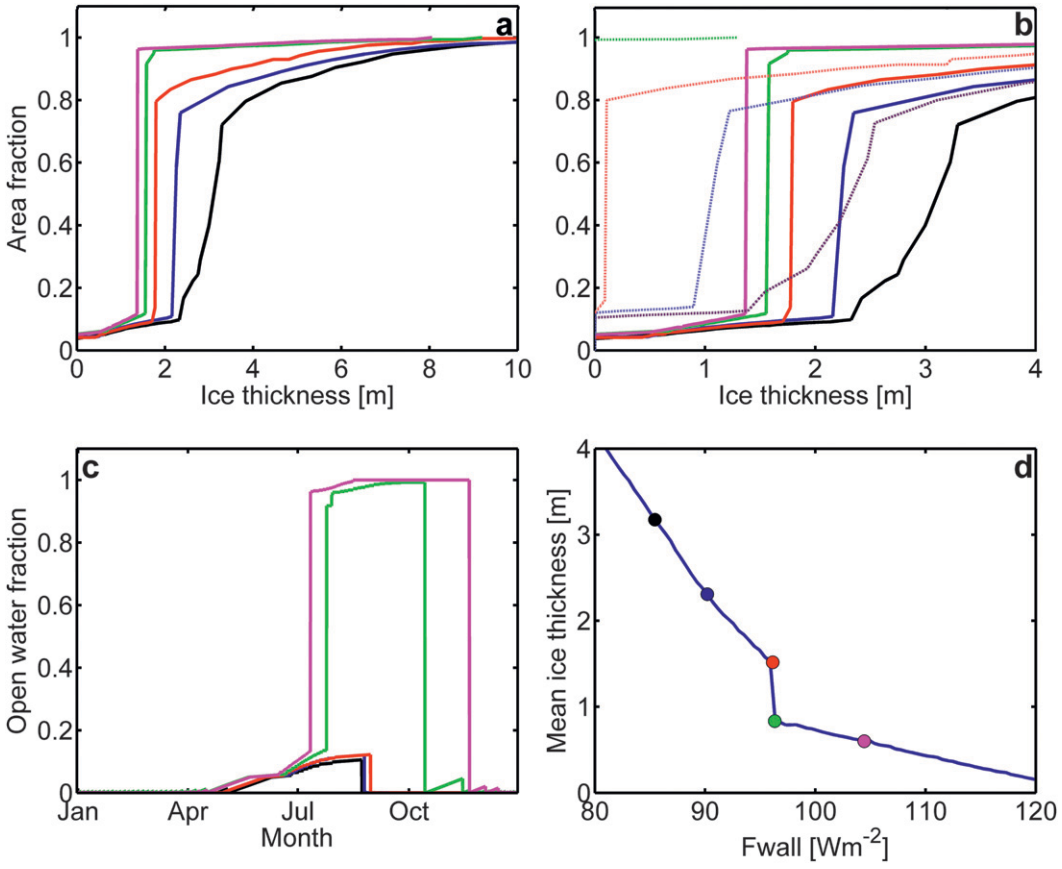

FIG. 3. Details of the transition from perennial ice to seasonal ice for different values of F_{wall} using the ECHAM5 albedo scheme. The color of filled circles for the ice thickness in (d) refers to curves in (a)–(c). (a) Cumulative thickness distribution for different values of F_{wall} at the time for maximal ice thickness during the year. (b) Cumulative thickness distribution for different values of F_{wall} at the time for maximum (solid curves) and minimum (dotted curves) ice thickness during the year. (c) Temporal evolution of the open water fraction over the year for different values of F_{wall}. (d) Annual-mean ice thickness as a function of F_{wall}.

thickness dependence (Fig. 1). The exceptionally thin ice for the CCSM3 albedo scheme is interesting since it shows clearly that the low albedo has to be compensated by other processes in order to generate a realistic ice thickness (or any ice at all) in the fully coupled global model runs. The CCSM3 is indeed known to give realistic ice thickness in GCM runs under present-day climate (Holland et al. 2010). This issue is further treated in section 4.

The sharp transition between the multiyear and the seasonal ice regime, which is characteristic for all albedo schemes (except the constant one), is caused by the interplay between ice thickness distribution and low open water albedo. An example of how the transition takes place in more detail is shown in Fig. 3, using the ECHAM5 albedo scheme. A general feature in these steady state runs is that the ice thickness distribution follows an annual cycle that is identical each year. The thickness distribution as a whole is, however, not in equilibrium with the thermodynamic forcing since the ice export demands a net ice growth. Another characteristic is that a specific annual ice thickness cycle (equilibrium cycle) exists for which the ice growth equals the ice melt each year. This corresponds to the cycle a single ice floe would follow if left undisturbed for long enough time in the basin. Ice that follows the equilibrium cycle is thus in a long-term thermodynamic equilibrium. An equilibrium ice thickness can then be defined for each time of the year. Ice thicker/thinner than the equilibrium cycle tends to reduce/increase its thickness toward the equilibrium. With respect to the thickness distribution, this means that there is a tendency to build up dominating ice categories occupying a large area fraction at the equilibrium thickness. In addition, there are processes that generate ice that is thicker and thinner than the equilibrium. Ice export

continuously creates open water that freezes into thin new ice, which then successively increases in thickness toward the equilibrium cycle. Ridging creates both open water and thick ice where the thick ice can be much thicker than the equilibrium thickness. The thick ice gradually reduces its thickness toward the equilibrium, while the new ice formed from open water increases in thickness. How dominant the categories near the equilibrium cycle become is controlled by the time scale for the adjustment process toward equilibrium and the residence time of the ice in the basin. If the residence time is long compared to the adjustment time scale, there will in general be a large amount of ice close to the equilibrium thickness, and vice versa. In our case the residence time is constant and about 7 yr ($1/D$, where D is the divergence rate). The adjustment time scale for thin new ice to reach the equilibrium is related to the mean ice thickness h_{ice} with longer time scale for thicker ice. Since h_{ice} decreases with increasing F_{wall}, the time scale then becomes shorter.

Figure 3a shows the cumulative ice thickness distribution at the time of the annual maximum ice thickness for some specific values of F_{wall} (see Fig. 3d). Starting at $F_{\text{wall}} \approx 86$ W m^{-2}, there are dominating ice categories around 3-m thickness (seen as the steep slope of the cumulative thickness distribution). Increasing F_{wall} to about 90 W m^{-2} gives very distinct and dominating categories at about 2.2 m occupying an area fraction of nearly 70%. Increasing F_{wall} further makes the equilibrium thickness even thinner, reduces the adjustment time scale, and makes the dominating category covering an even greater area fraction. Figure 3b shows the ice thickness distribution both at the time of the maximum and minimum mean ice thickness h'_{ice} and with a different thickness scale focusing on the thinner part of the distribution. The thickness of the dominant ice category for minimum ice conditions approaches zero more rapidly than for the maximum conditions when increasing F_{wall}. It is about 1 m for $F_{\text{wall}} \approx 90$ W m^{-2} (dashed blue curve) and less than 10 cm for the point just before the transition (dashed red curve). When increasing F_{wall} slightly more (dashed green) this category melts completely during summer and the model enters a nearly seasonal state directly. The ice thickness decreases here in a steplike fashion (Fig. 3d), which is a result of the surface albedo feedback. As soon as the dominating category melts completely, there is no possibility to maintain an equilibrium cycle with just a few days of open water because, when this large area fraction becomes ice free, the albedo will be lowered significantly and enhance the amount of solar radiation absorbed by the ocean. The final thickness of the first year ice produced from this open water will then be smaller and will melt somewhat earlier in the season, which will further enhance the oceanic absorption and so on. The system has then to find a new equilibrium characterized by a quite long period of almost completely open water during summer (a few very thick ridged ice categories will still survive the summer but these occupy only a very small area fraction). During the open water period the upper ocean will warm, followed by cooling toward the freezing point during fall and then ice growth to significantly thinner ice at the end of winter. This is clearly seen in Fig. 3c showing that the open water fraction increases largely both in time and amount for just an incremental increase of F_{wall} (red and green curves). When increasing F_{wall} beyond the threshold the system has a more linear response with a successive increase in length of the ice free period (green and magenta curves).

Note the relatively linear thickness response on F_{wall} in the perennial regime, which is rather typical for this kind of model and is a result of the constant divergence (or areal ice export) giving rise to a negative ice thickness–ice volume export feedback [for further discussion of this feedback, see Stranne and Björk (2012)].

b. Response to changes in F_{wall} and F_{SW}

The other major forcing factor of the Arctic ice cover is the solar radiation. The annual-mean incident solar radiation at the top of the atmosphere (F_{SW}) varies significantly over the Arctic Ocean latitudes ranging from about 210 W m^{-2} at 65°N (roughly the latitude of Bering Strait) to less than 175 W m^{-2} at the North Pole. This range of more than 30 W m^{-2} can be expected to have a large impact on ice conditions. It is rather straightforward to test the effect of varying solar radiation in the present model by simply changing the latitude in the radiation module. The model results can then be interpreted as representing a small area around a specific latitude. We then make the assumption that the ocean stratification, ice divergence, and atmospheric properties are similar over the entire basin. Since F_{wall} and F_{SW} have about equal weights in the Arctic heat budget, it is natural to run the sensitivity studies over a two-dimensional space giving ice thickness response fields instead of curves for the different albedo schemes.

In general, the amount of solar radiation has a large effect on the ice thickness, as can be seen from the sloping isolines of ice thickness, but again the exact behavior is very much dependent on the albedo scheme (Fig. 4). Note that the narrow transition between perennial and seasonal ice is rather evident in these figures as a band with closely spaced isolines (or a bold

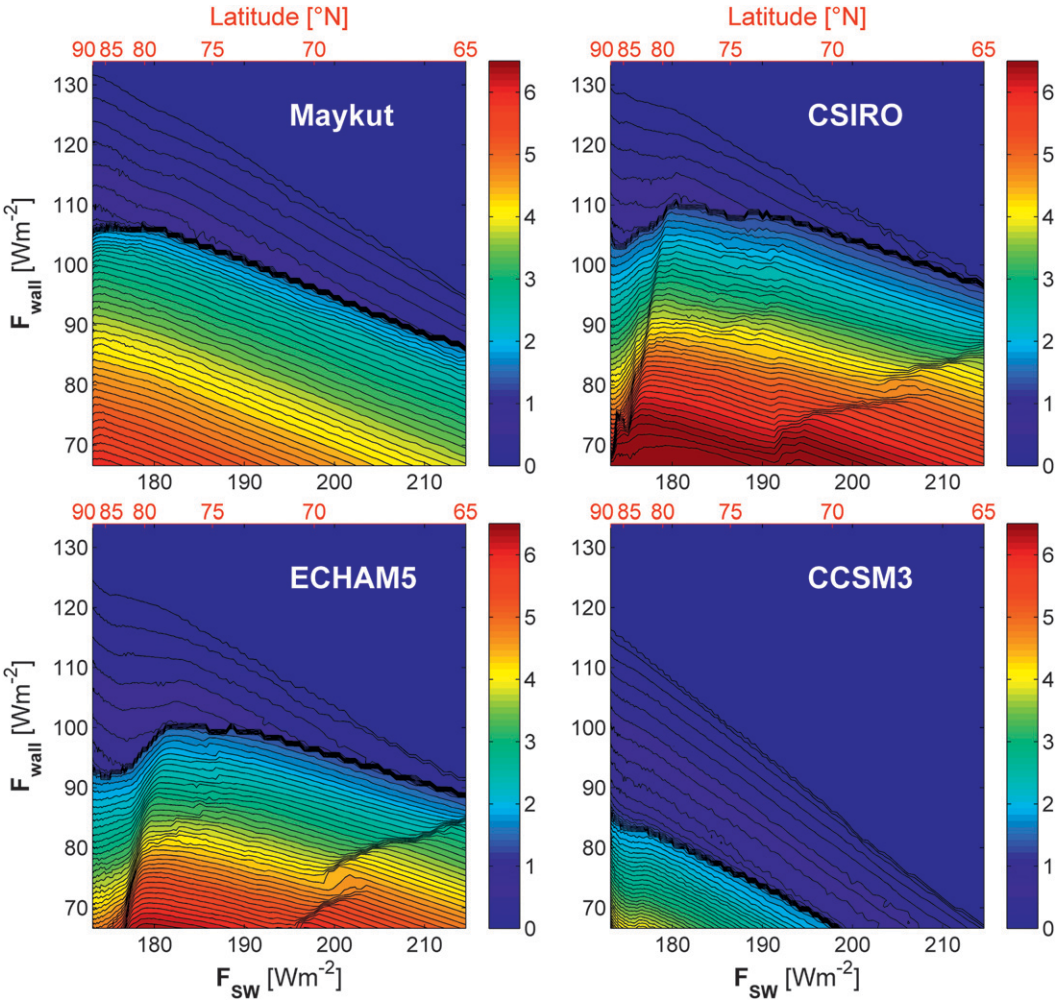

FIG. 4. Response fields showing the mean ice thickness h_{ice} (m) as a function of F_{wall} and F_{SW} for different types of albedo parameterizations. Bold black lines (or actually tightly spaced isolines) mark the transition between perennial and seasonal ice regimes.

black line). Ice free conditions are represented by a constant dark blue color at the upper right side of each panel. The annual-mean solar radiation F_{SW} is directly related to latitude as shown by the separate scale at the top of each panel.

The Maykut albedo scheme gives the most regular field where the ice thickness is a nearly linear function of F_{wall} and F_{SW} in the perennial regime, with $dh_{ice}/dF_{wall} \approx 0.1$ m (W m^{-2})$^{-1}$ and $dh_{ice}/dF_{SW} \approx 0.05$ m (W m^{-2})$^{-1}$. The sensitivity to F_{wall} is thus twice the sensitivity to F_{SW}, which is natural since a large fraction of the solar radiation is reflected back to space by the clouds, prescribed by CF and CWP (see section 2a and Table 1) and the surface albedo. The transition between perennial and seasonal ice follows mostly a straight line across the F_{wall}–F_{SW} plane except for low values of solar insolation. Assuming 100 W m^{-2} as a typical value for F_{wall} there is perennial ice for F_{SW} less than about 192 W m^{-2} or, equivalently, north of 73°N. This corresponds to the Siberian Shelf seas, Chukchi Sea, and southern Beaufort Sea having seasonal ice, which, in fact, is a quite realistic representation of the typical Arctic ice cover.

Both CSIRO and ECHAM5 schemes give similar but more irregular response fields. The main difference between the two is that the perennial ice regime is present for higher values of F_{wall} for the CSIRO as seen earlier. Using, again, $F_{wall} = 100$ W m^{-2} as a typical value the model is not able to reproduce any perennial ice at all with the ECHAM5 albedo scheme, while with CSIRO perennial ice is formed over most of the domain all the way down to 66°N. The perennial regime has a nearly linear dependence on both variables for $F_{SW} > \sim 180$ W m^{-2}, which is similar to the Maykut scheme.

A specific feature is that the ice thickness tends to decrease for low values of F_{SW} corresponding to high latitudes above 80°N. The reason for this is that the diurnal cycle of solar radiation gets weaker close to the pole, which has a strong impact on the snow cover during summer in the model. At lower latitudes, where the diurnal cycle is more pronounced, the snow is able to accumulate during night when the surface temperature goes below zero. This will not happen near the North Pole, where the diurnal cycle is smaller and where melting conditions prevail over the entire day and prevents the snow from accumulating even though the total F_{SW} is smaller. At lower latitudes, where the snow accumulates overnight, it takes some time during the morning to melt it away, especially since the snow albedo is rather high. The total time period of the day available for melting ice will be reduced, giving less total melting over the summer compared to the highest latitudes, which then results in thicker ice. It is of course questionable how realistic this effect is since the precipitation, in realty, is not constant but has large regional and temporal variability.

Another feature is the sudden jump of the ice thickness at the lower right of the CSIRO and ECHAM5 fields. This transition is also related to the diurnal cycle of shortwave (SW) forcing through nighttime freezing of open water at lower latitudes (or small F_{wall}), while no freezing occurs during night at higher latitudes (or larger F_{wall}). Since these two albedo parameterizations do not include a thickness-dependent ice surface albedo, there is a substantial albedo contrast between ice and open water even for very thin new ice. This effect is not present for the Maykut and CCSM3 albedo schemes since they have a gradually decreasing albedo with decreasing ice thickness toward the open water value.

The relatively dark CCSM3 albedo gives perennial ice only for F_{SW} less than about 197 W m^{-2} and F_{wall} not larger than 85 W m^{-2}. Interestingly the transition line between seasonal ice and ice-free conditions is located not much different from for example ECHAM5. This can be explained by the generally smaller model sensitivity to forcing changes in the seasonal ice regime.

c. *Snow precipitation sensitivity*

Snow cover plays an important role for the thermodynamic properties of the ice cover. Snow insulates ice from losing heat to the atmosphere and therefore reduces ice growth during winter (insulating effect) and prolongs the surface melting later into summer by increasing the albedo (whitening effect). The snow cover also acts as a barrier, which has to be melted away first before the surface melting of the ice can start (barrier effect). Both the whitening and barrier effects tend to reduce melting during summer. Since the snow is actively coupled to the surface albedo, it is actually the combination of surface albedo formulation together with the amounts of snow precipitation that determines the effective albedo of the ice cover. The combined effect of snow precipitation and type of albedo parameterization is shown in Fig. 5.

For constant surface albedo the snow acts only as an insulating layer and decreases the ice thickness. The other albedo schemes have rather different response properties for different amount of snow precipitation. The Maykut and CSIRO schemes give a relatively similar snow response with generally thicker ice when adding snow, but the actual amount of precipitation is not so important. Adding just a thin layer of snow will have a large effect by increasing the albedo without providing much insulation. Below $F_{wall} = 100$ W m^{-2} all three cases of snow precipitation fall almost on the same curve. The insulating effect of adding more snow is then nearly exactly compensated by the whitening and barrier effect of snow. Near the transition to seasonal ice the amount of snowfall has some effect such that the 0.5 case gives transition to seasonal ice for the highest F_{wall}. This is because the insulating effect tends to be more efficient for thin ice since the snow then becomes more dominating in controlling the overall heat conduction from the bottom of the ice to the top of the snow cover.

The ECHAM5 albedo scheme gives a different snow response with gradually decreasing ice thickness with increasing snow over most of the F_{wall} range. This can be explained by the ECHAM5 snow albedo being generally lower compared to the other types. It is low enough such that the insulating effect typically dominates over the whitening effect.

The CCSM3 albedo scheme has yet another type of response with gradually increasing ice thickness with amount of snow precipitation. This behavior is caused by the snow depth-dependent albedo formulation. More snow gives generally a higher albedo and thus reduces the summer melt, which in turn results in thicker ice. This effect is most active when the snow cover is relatively thin (<20 cm, according to Fig. 1). Having a thicker snowpack will move the date when snow becomes thin enough to enter the thickness-dependent albedo regime later into the summer that gives an increase of the overall summer albedo and reduced melting.

4. Discussion

This study shows that, regardless of which albedo parameterization is being employed (except the constant one), the transition into seasonal ice, due to the

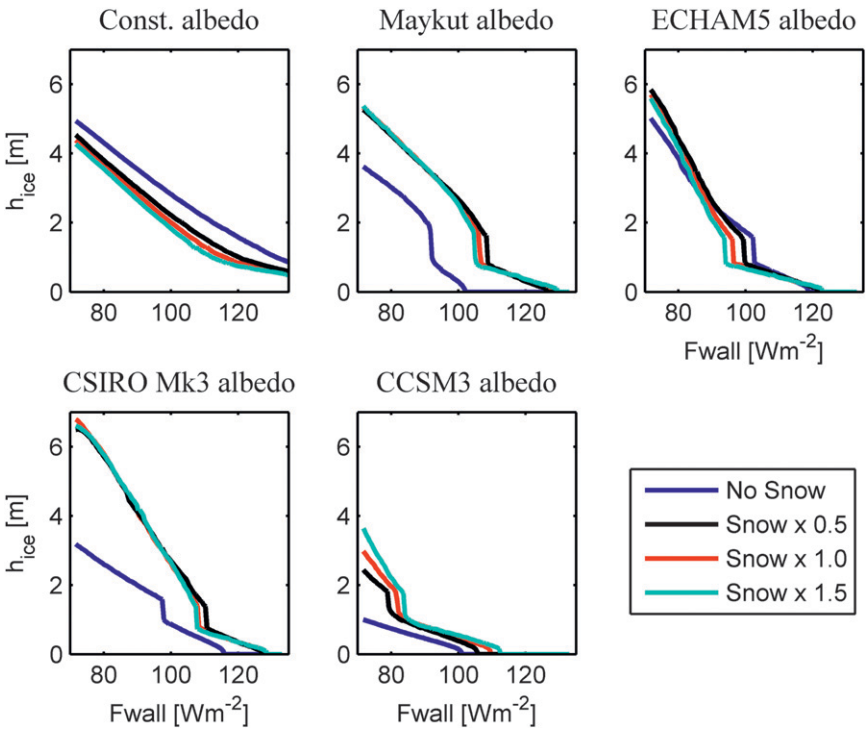

FIG. 5. Response curves for different amounts of snow precipitation using different albedo parameterizations. Snow × 1.0 is for the standard case.

surface albedo feedback, is abrupt and occurs at a critical mean ice thickness h_{ice} of around 1.7–2.0 m. When it comes to the sensitivity of the perennial ice cover to changes in the external forcing, it is then important how close the ice cover is to the threshold. When the ice thickness is near the threshold, it can be expected that just a small positive forcing perturbation in, for example, F_{wall} can force the ice into the seasonal regime. Hence, a perennial ice cover should be more stable to negative perturbations where the ice thickness will basically increase linearly in response to forcing changes. In a climatic perspective with a gradually decreasing ice thickness from about 3.5 m in the 1970s, as shown by observations, this implies that the ice cover has become more and more sensitive to positive forcing perturbations as it approaches the critical thickness of about 2 m.

This type of sensitivity is also dependent on geographical location, or more specific on latitude, owing to the tendency to have thinner ice at lower latitudes because of larger solar insolation. For example, the ice thickness along the Siberian coast is typically thinner than in the central Arctic (Kwok et al. 2009) and should therefore also be more vulnerable to increased thermodynamic forcing. As a consequence, typical temporal and regional variations in the thermal forcing should be able to cause large temporal and regional variations of the latitudinal extent of the perennial ice on interannual time scales. This is also a well-known feature of the Arctic pack ice, which becomes evident from satellite observations of the areal ice cover extent (Parkinson and Cavalieri 2008). It is also possible that the recent dramatic decrease of ice extent and associated large areas of seasonal ice, especially since summer 2007, can be a result of a relatively small increase of the atmospheric thermodynamic forcing in combination with high sensitivity close to the critical ice thickness. This reasoning, offers a complimentary explanation to the observed sea ice reduction in addition to other suggested causes such as reduction of cloudiness (Kay et al. 2008), enhanced ice export (Kwok et al. 2009), anomalously strong southerly winds (Comiso et al. 2008), increased atmospheric energy transport (Graversen et al. 2008), and increased oceanic heat fluxes (Shimada et al. 2006). It is also in line with the abrupt reductions of sea ice cover seen in twenty-first-century climate model simulations, which may be related to a large summer melting that takes place when a critical ice thickness is reached (Holland et al. 2006).

The behavior of the transition from perennial ice to seasonal ice is very much dependent on the model formulation. Using a more idealized model, Eisenman and

Wettlaufer (2009) show that the ice cover can, indeed, develop from perennial ice to seasonal ice when increasing the thermal forcing as long as nonlinear sea ice thermodynamic effects are included in the model. However, the transition between perennial and seasonal ice is smooth in their study with no steplike behavior of the ice thickness at the transition, as is the case here. This is likely due to the fact that the idealized model just includes one single ice type and has a rather smooth albedo dependence on ice thickness. In our model, this is contrasted by the development of a large category of thin ice near the transition that gives a transient shift of the overall albedo when it finally melts, which in turn triggers an albedo feedback leading to a significantly prolonged open water season.

This study only includes effects of horizontal variations in terms of latitudinal changes of solar insolation that tend to give thicker ice toward the pole. Superimposed on this tendency there might, in reality, be horizontal variations of other properties that are not resolved in a one-dimensional (1D) column model, giving a different ice thickness–latitude relationship. For instance, there might be systematic latitudinal variations in cloudiness that could counteract the effect of solar radiation. Horizontal differences in the wind field can force the ice cover to become more compact and thicker at specific locations (as indeed is the case north of Greenland) or generate large areas of open water at leeward coasts, especially during summer. Such effects must be investigated using a 2D ice model that includes a realistic wind field. Although hard to compare directly, investigations using a 2D dynamic–thermodynamic ice model with prescribed atmospheric forcing (Liu et al. 2007) show large differences in ice thickness for the different albedo schemes in qualitative agreement with the present study. In their study, the CCSM3 albedo gives a June–September ice thickness of 0.2–0.8 m over the most part of the basin while a higher albedo of 0.75 (corresponding best to the ECHAM5 albedo in our study) gives a thickness in the range 1–3 m over the same area.

Using different albedo parameterizations but keeping everything else the same as in our model experiments results in large differences of the ice thickness (Fig. 4). Choosing $F_{\text{wall}} = 100$ W m^{-2}, which is a realistic baseline value, implies that the CSIRO albedo scheme generates perennial ice with 2.3–2.8-m thickness over most of the latitude band, while the ECHAM5 and particularly the CCSM3 albedo schemes are not able to produce any perennial ice at all. This suggests that there are compensating effects when these schemes are used in the full GCMs since all three models produce a perennial ice cover for late-twentieth-century simulations (Holland et al. 2010). In fact, the CCSM3 and ECHAM5 GCMs both produce an ice cover with a thickness of more than 3 m in the central Arctic Ocean. There are indeed large intermodel differences of quantities important for the energy balance such as cloudiness and downward longwave radiation. For instance, the GCM intermodel scatter of winter cloud fraction spans between 40% and 90% (Eisenman et al. 2007).

As another example of a possibly important compensating factor we focus on the cloud properties. As shown by Gorodetskaya et al. (2008), the SW cloud forcing (SCF) in the CCSM3 is significantly larger compared to other models during twentieth-century simulations. A large SCF results in less SW radiation reaching the surface, and the CCSM3 should then produce thicker ice compared to other models if everything else is the same. The Arctic clouds in CCSM3 absorb and reflect 60 W m^{-2} more of the SW radiation in June compared to the Goddard Institute for Space Studies Model E-R (GISS-ER) and about 40 W m^{-2} more than the HadCM3. This makes a quite significant difference in terms of the surface radiation budget. If, on the other hand, the albedo is lower in the CCSM3 compared to other models, as in fact it is, one can expect that these two effects will cancel each other out to some degree.

The two main parameters controlling the SCF are the cloud fraction (CF) and cloud water path (CWP), where the CWP is the dominating factor (Gorodetskaya et al. 2008). To quantify how increased cloud forcing affects the ice thickness using the CCSM3 albedo formulation, we increase the CWP so that it reaches a maximum of 200 g m^{-2} in summer, a value similar to the actual CWP in the CCSM3 during twentieth-century simulations. This is a relatively high value compared to observational estimates of around 100 g m^{-2} (Gorodetskaya et al. 2008). The increased CWP generates a significantly thicker ice cover, as expected (Fig. 6), and the maximum thickness is now similar to the other albedo schemes, in Fig. 4, run with considerably less CWP. Note, however, that the CCSM3 scheme is still not able to generate any perennial ice for $F_{\text{wall}} = 100$ W m^{-2}. This suggests that there are still other compensating mechanisms at work in the full CCSM3 climate simulations, such as other cloud parameters than CWP or that F_{wall} is typically lower than 100 W m^{-2}. There are also possible compensations related to ice dynamics and oceanic heat flux.

Another important aspect in this context is how sensitive the model is to changes in the surface albedo. Pure thermodynamic ice models including one single ice type are generally extremely sensitive to albedo changes due to the strong ice thickness–ice growth rate feedback mechanism. For example, Eisenman et al. (2007) show an ice thickness change from 2 to 6 m for a 0.08 albedo

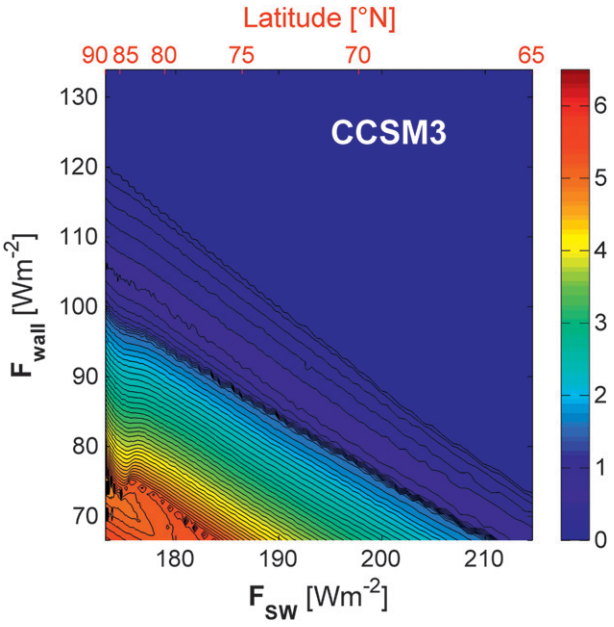

FIG. 6. As in Fig. 4c but with enhanced cloud water path; see text for details.

change. The sensitivity is smaller in our model where the ice export imposes a strong negative feedback, giving a much more linear response in the perennial ice regime (Stranne and Björk 2012). A rough estimate of the albedo sensitivity can be obtained by comparing CSIRO and ECHAM5 schemes having a difference of about 0.07 units at 0°C (Fig. 1). The difference in thickness for $F_{\text{wall}} = 90$ W m^{-2} between these albedos is typically 1.5 m in the present model. In the full GCM runs the albedo sensitivity can be further reduced as shown for the CCSM3 for which an albedo increase of 0.08 gives a thickness increase of 0.65 m from 1.95 to 2.5 m (DeWeaver et al. 2008). The smaller sensitivity in the CCSM3 climate model is then attributed to changes in the cloud fraction and effects of multiple scattering in clouds.

In this study the cloud fraction, the liquid water path, and the atmospheric water vapor content and vertical distribution follow annual climatological cycles, which means that the associated local cloud formation and water vapor feedbacks are not taken into consideration. It would therefore be valuable to include active water vapor cloud and dynamics in this type of sensitivity studies. The parameterizations of these processes give varying results however and are currently under debate (e.g., Verlinde et al. 2007; Soden and Held 2006).

Related to the cloud formation and cloud feedback is the precipitation. In the present approach the snow precipitation is continuous and handled so that snow is accumulating as long as the air surface temperature is below zero (otherwise, a corresponding amount of liquid water is added to the ocean mixed layer). The continuous snow precipitation in combination with the surface albedo feedback and the latitude dependence of the diurnal cycle of F_{SW} has a quite large impact on the ice thickness. Although this is possibly an interesting effect, it would be preferable to test the robustness by using a more intermittent type of snow precipitation, as in the study by Schramm et al. (1997), and also a more sophisticated snow modeling scheme including, for example, dependence of crystal size due to snow temperature and age, which has been shown to be important (e.g., Cheng et al. 2008).

Note that we investigate the steady-state response; that is, the model spins up over 50 years for each type of forcing and model setup, and the resulting constant annually repetitive cycles from the end of the simulation are stored and used for output of specific quantities such as annual-mean, maximum, and minimum ice thickness. In reality, the Arctic pack ice strives to adapt to the forcing but never quite reaches a steady state since the forcing is constantly shifting on time scales smaller than the adjustment time scales of the ice cover. Since the climate system is all but linear, it is possible that the response properties for a more realistic and stochastic type of forcing with random anomalies superimposed upon the regular annual cycles can be different from the mean forcing responses and also introduce low frequency variability (L'Hévéder and Houssais 2001). To estimate the effect of nonlinearities in combination with random forcing, we suggest running the same type of model over much longer time periods (~1000 yr) and with various types of random forcing fluctuations.

5. Conclusions

This study shows that the type of albedo parameterization is important not only for the ice thickness itself but also for the response properties of the ice cover to climatic changes. For climatic scenario runs it seems to be critical how close the model is to the transition to seasonal ice, which in turn depends on the albedo formulation. Another important aspect is that different albedo parameterizations give rather different ice thickness–snow precipitation responses. This brings an extra complication to global climate models having, in addition, different moisture transports and associated changes in precipitation.

Acknowledgments. This work was funded by the EU project DAMOCLES (Contract 018509), the Swedish Research Council (Contract 621-2007-3836), and the

Research Platform TELLUS at University of Gothenburg. We thank three anonymous reviewers, whose suggestions helped to improve the paper.

APPENDIX

Detailed Description of Albedo Schemes

Each ice category has its own ice thickness H_{ice} (same as H_i in the expression for mean ice thickness), surface temperature T_s, and snow depth H_{snow}, and the albedo is calculated separately for each individual ice category using the albedo schemes presented below. The index notation i for each category is thus dropped in the expressions below for simplicity.

a. Maykut albedo scheme

The Maykut albedo parameterization (Maykut 1982) is a function of surface type (open water, bare ice, or snow covered) and ice thickness. The snow albedo follows a prescribed annual cycle (see Table 1). The bare ice albedo α is a function of ice thickness following

$$\alpha = \min(0.08 + 0.44H_{\text{ice}}^{0.28}, 0.64),$$

which also gives the open water albedo for $H_{\text{ice}} = 0$.

b. ECHAM5 albedo scheme

The ECHAM5 albedo parameterization (Roeckner et al. 2003) is a function of surface type (open water, bare ice, or snow covered) and surface temperature:

$$\alpha = \begin{cases} \alpha i_{\min} + (\alpha i_{\max} - \alpha i_{\min})f, & \text{bare ice} \\ \alpha s_{\min} + (\alpha s_{\max} - \alpha s_{\min})f, & \text{snow covered} \\ 0.07, & \text{open water} \end{cases}$$

with

$$f = \min\{\max[(T_m - T_s)/(T_m - T_d), 0], 1\}$$

and

$$T_d = T_m - 1,$$

where $\alpha i_{\min} = 0.50$ (minimum albedo for sea ice), $\alpha i_{\max} = 0.75$ (maximum albedo for sea ice), $\alpha s_{\min} = 0.60$ (minimum snow albedo), $\alpha s_{\max} = 0.80$ (maximum snow albedo), T_s = surface temperature, and T_m = melting point.

c. CSIRO Mk3 albedo scheme

The CSIRO Mk3 albedo parameterization (Gordon et al. 2002) is a function of surface type (open water, bare ice, or snow covered), surface temperature, and solar zenith angle z_r.

The open water albedo is a function of solar zenith angle:

$$\alpha = 0.05/\{0.15 + \text{abs}[\cos(z_r)]\}.$$

For bare ice

$$\alpha = \begin{cases} 0.65, & T_s < 0 \\ 0.55, & T_s \geq 0 \end{cases}$$

and for snow covered ice

$$\alpha = \begin{cases} 0.80, & T_s < 0 \\ 0.70, & T_s \geq 0. \end{cases}$$

d. CCSM3 albedo scheme

The CCSM3 albedo parameterization (Briegleb et al. 2004) depends on surface type (open water, bare ice, or snow covered), ice thickness, snow depth, surface temperature, and spectral bands (the ratio is a function of CWP and solar zenith angle). Here the snow and ice spectral albedos (visible = vs, wavelength < 0.7 μm, near infrared = ni and wavelength > 0.7 μm) are distinguished. The dry snow spectral albedos are

$$\alpha_{\text{vs}}^s(\text{dry}) = 0.96 \quad \alpha_{\text{ni}}^s(\text{dry}) = 0.68$$

To represent melting snow albedo, the surface temperature T_s is used. If $T_s \geq -1$°C, then

$$\Delta T_s = T_s + 1.0 \quad \alpha_{\text{vs}}^s(\text{melt}) = \alpha_{\text{vs}}^s(\text{dry}) - 0.10\Delta T_s$$
$$\alpha_{\text{ni}}^s(\text{melt}) = \alpha_{\text{ni}}^s(\text{dry}) - 0.15\Delta T_s.$$

For bare nonmelting sea ice, the albedo depends on ice thickness and spectral band. If $H_{\text{ice}} < 0.5$ m, then

$$\alpha_{\text{vs}}(\text{dry}) = \alpha_0(1 - f_h) + \alpha_{\text{vs}}(\text{thick})f_h$$
$$\alpha_{\text{ni}}(\text{dry}) = \alpha_0(1 - f_h) + \alpha_{\text{ni}}(\text{thick})f_h,$$

where α_0 is the open water albedo ($\alpha_0 = 0.06$), and

$$f_h = \min[\tan^{-1}(c_{f_h} H_{ice})/\tan^{-1}(c_{f_h} 0.5), 1.0],$$

with $c_{fh} = 4$. The albedos for thick, nonmelting sea ice are

$$\alpha_{\text{vs}}(\text{thick}) = 0.73 \quad \alpha_{\text{ni}}(\text{thick}) = 0.33.$$

For bare melting sea ice the albedo is reduced in order to crudely approximate melt ponds. If $T_s \geq -1°C$, then

$$\alpha_{vs}(\text{melt}) = \alpha_{vs}(\text{dry}) - 0.075\Delta T_s$$
$$\alpha_{ni}(\text{melt}) = \alpha^s_{ni}(\text{dry}) - 0.075\Delta T_s.$$

The horizontal fraction of the surface covered with snow is a function of snow depth H_{snow} according to

$$f_s = \frac{H_{\text{snow}}}{H_{\text{snow}} + \text{snowpatch}},$$

where snowpatch = 0.02. The combined surface albedo for each ice thickness category is then given by

$$\alpha_{vs} = \alpha_{vs}(1 - f_s) + f_s\alpha^s_{vs}$$
$$\alpha_{ni} = \alpha_{ni}(1 - f_s) + f_s\alpha^s_{ni}.$$

REFERENCES

Arctic Climatology Project, 2000: *Environmental Working Group Arctic Meteorology and Climate Atlas.* F. Fetterer and V. Radionov, Eds., National Snow and Ice Data Center, CD-ROM.

Björk, G., 1989: A one-dimensional model for the vertical stratification of the upper Arctic Ocean. *J. Phys. Oceanogr.,* **19,** 52–67.

——, 1997: The relation between ice deformation oceanic heat flux and the ice thickness distribution in the Arctic Ocean. *J. Geophys. Res.,* **102** (C8), 18 681–18 698.

——, and J. Söderkvist, 2002: Dependence of the Arctic Ocean ice thickness distribution on the poleward energy flux in the atmosphere. *J. Geophys. Res.,* **107,** 3173, doi:10.1029/2000JC000723.

Briegleb, B. P., C. M. Bitz, E. C. Hunke, W. H. Lipscomb, M. M. Holland, J. L. Schramm, and R. E. Moritz, 2004: Scientific description of the sea ice component in the Community Climate System Model, version three. NCAR Tech. Note NCAR/TN-463+STR, 78 pp.

Cheng, B., Z. Zhang, T. Vihma, M. Johansson, L. Bian, Z. Li, and H. Wu, 2008: Model experiments on snow and ice thermodynamics in the Arctic Ocean with CHINARE 2003 data. *J. Geophys. Res.,* **113,** C09020, doi:10.1029/2007JC004654.

Collins, W. D., and Coauthors, 2006: The Community Climate System Model version 3 (CCSM3). *J. Climate,* **19,** 2122–2143.

Comiso, J. C., C. L. Parkinson, R. Gersten, and L. Stock, 2008: Accelerated decline in the Arctic sea ice cover. *Geophys. Res. Lett.,* **35,** L01703, doi:10.1029/2007GL031972.

Curry, J. A., J. L. Schramm, and E. E. Ebert, 1995: Sea ice–albedo climate feedback mechanism. *J. Climate,* **8,** 240–247.

DeWeaver, E. T., E. C. Hunke, and M. M. Holland, 2008: Comment on ''On the reliability of simulated Arctic sea ice in global climate models'' by I. Eisenman, N. Untersteiner, and J. S. Wettlaufer. *Geophys. Res. Lett.,* **35,** L04501, doi:10.1029/2007GL031325.

Eisenman, I., and J. S. Wettlaufer, 2009: Nonlinear threshold behavior during the loss of Arctic sea ice. *Proc. Natl. Acad. Sci. USA,* **106,** 28–32, doi:10.1073/pnas.0806887106.

——, N. Untersteiner, and J. S. Wettlaufer, 2007: On the reliability of simulated Arctic sea ice in global climate models. *Geophys. Res. Lett.,* **34,** L10501, doi:10.1029/2007GL029914.

Gordon, H. B., and Coauthors, 2002: The CSIRO Mk3 climate system model. CSIRO Atmospheric Research Tech. Paper 60, 134 pp.

Gorodetskaya, I. V., L.-B. Tremblay, B. Liepert, M. A. Cane, and R. I. Cullather, 2008: The influence of cloud and surface properties on the Arctic Ocean shortwave radiation budget in coupled models. *J. Climate,* **21,** 866–882.

Graversen, R. G., T. Mauritsen, M. Tjernström, E. Källén, and G. Svensson, 2008: Vertical structure of the recent Arctic warming. *Nature,* **541,** 53–56, doi:10.1038/nature06502.

Holland, M. M., and J. A. Curry, 1999: The role of physical processes in determining the interdecadal variability of central Arctic sea ice. *J. Climate,* **12,** 3319–3330.

——, C. M. Bitz, and B. Tremblay, 2006: Future abrupt reductions in the summer Arctic sea ice. *Geophys. Res. Lett.,* **33,** L23503, doi:10.1029/2006GL028024.

——, M. C. Serreze, and J. Stroeve, 2010: The sea ice mass budget of the Arctic and its future change as simulated by coupled climate models. *Climate Dyn.,* **34,** 185–200, doi:10.1007/s00382-008-0493-4.

Houghton, J. T., Y. Ding, D. J. Griggs, M. Noguer, P. J. van der Linden, X. Dai, K. Maskell, and C. A. Johnson, Eds., 2001: *Climate Change 2001: The Scientific Basis.* Cambridge University Press, 881 pp.

Kay, J. E., T. L'Ecuyer, A. Gettelman, G. Stephens, and C. O'Dell, 2008: The contribution of cloud and radiation anomalies to the 2007 Arctic sea ice extent minimum. *J. Geophys. Res.,* **35,** L08503, doi:10.1029/2008GL033451.

Kwok, R., 2011: Observational assessment of Arctic Ocean sea ice motion, export, and thickness in CMIP3 climate simulations. *J. Geophys. Res.,* **116,** C00D05, doi:10.1029/2011JC007004.

——, and D. A. Rothrock, 1999: Variability of Fram Strait ice flux and North Atlantic Oscillation. *J. Geophys. Res.,* **104** (C3), 5177–5189.

——, G. F. Cunningham, M. Wensnahan, I. Rigor, H. J. Zwally, and D. Yi, 2009: Thinning and volume loss of the Arctic Ocean sea ice cover: 2003–2008. *J. Geophys. Res.,* **114,** C07005, doi:10.1029/2009JC005312.

L'Hévéder, B., and M.-N. Houssais, 2001: Investigating the variability of the Arctic sea ice thickness in response to a stochastic thermodynamic atmospheric forcing. *Climate Dyn.,* **17,** 107–125.

Liu, J., Z. Zhang, J. Inoued, and R. M. Hortone, 2007: Evaluation of snow/ice albedo parameterizations and their impacts on sea ice simulations. *Int. J. Climatol.,* **27,** 81–91, doi:10.1002/joc.1373.

Maslanik, J. A., C. Fowler, J. Stroeve, S. Drobot, J. Zwally, D. Yi, and W. Emery, 2007: A younger, thinner Arctic ice cover: Increased potential for rapid, extensive sea-ice loss. *Geophys. Res. Lett.,* **34,** L24501, doi:10.1029/2007GL032043.

Maykut, G. A., 1982: Large-scale heat exchange and ice production in the central Arctic. *J. Geophys. Res.,* **87** (C10), 7971–7984.

Meehl, G. A., C. Covey, T. Delworth, M. Latif, B. McAvaney, J. F. B. Mitchell, R. Stouffer, and K. E. Taylor, 2007: The WCRP CMIP3 multimodel dataset: A new era in climate change research. *Bull. Amer. Meteor. Soc.,* **88,** 1383–1394.

Overland, J. E., and P. Turet, 1994: Variability of the atmospheric energy flux across 70°N computed from the GFDL data set. *The Polar Oceans and Their Role in Shaping the Global Environment, Geophys. Monogr.,* Vol. 85, Amer. Geophys. Union, 313–325.

Parkinson, C. L., and D. J. Cavalieri, 2008: Arctic sea ice variability and trends. 1979–2006. *J. Geophys. Res.,* **113,** C07003, doi:10.1029/2007JC004558.

Perovich, D. K., and A. Richter-Menge, 2009: Loss of sea ice in the Arctic. *Annu. Rev. Mar. Sci.,* **1,** 417–441.

Polyakov, I. V., and Coauthors, 2010: Arctic Ocean warming contributes to reduced polar ice cap. *J. Phys. Oceanogr.,* **40,** 2743–2756.

Rinke, A., and Coauthors, 2006: Evaluation of an ensemble of Arctic regional climate models: Spatiotemporal fields during the SHEBA year. *Climate Dyn.,* **26,** 459–472, doi:10.1007/s00382-005-0095-3.

Roeckner, E., and Coauthors, 2003: The atmospheric general circulation model ECHAM5: Part I. Max Planck Institute for Meteorology Rep. 349, 140 pp.

Rossow, W. B., and E. N. Duenas, 2004: The International Satellite Cloud Climatology Project (ISCCP) web site: An online resource for research. *Bull. Amer. Meteor. Soc.,* **85,** 167–172.

Rothrock, D. A., D. B. Percival, and M. Wensnahan, 2008: The decline in Arctic sea-ice thickness: Separating the spatial, annual, and interannual variability in a quarter century of submarine data. *J. Geophys. Res.,* **113,** C05003, doi:10.1029/2007JC004252.

Schramm, J. L., M. M. Holland, and J. A. Curry, 1997: The effects of snowfall on a snow-ice-thickness distribution. *Ann. Glaciol.,* **25,** 287–291.

Serreze, M. C., A. P. Barrett, A. G. Slater, M. Steele, J. Zhang, and K. E. Trenberth, 2007a: The large-scale energy budget of the Arctic. *J. Geophys. Res.,* **112,** D11122, doi:10.1029/2006JD008230.

——, M. M. Holland, and J. Stroeve, 2007b: Perspectives on the Arctic's shrinking sea-ice cover. *Science,* **315,** 1533–1536, doi:10.1126/science.1139426.

Shimada, K., T. Kamoshida, M. Itoh, S. Nishino, E. Carmack, F. A. McLaughlin, S. Zimmermann, and A. Proshutinsky, 2006: Pacific Ocean inflow: Influence on catastrophic reduction of sea ice cover in the Arctic Ocean. *Geophys. Res. Lett.,* **33,** L08605, doi:10.1029/2005GL025624.

Soden, B. J., and I. M. Held, 2006: An assessment of climate feedbacks in coupled ocean–atmosphere models. *J. Climate,* **19,** 3354–3360.

Stranne, C., and G. Björk, 2012: On the Arctic Ocean ice thickness response to changes in the external forcing. *Climate Dyn.,* **39,** 3007–3018, doi:10.1007/s00382-011-1275-y.

Thorndike, A., 1992: A toy model linking atmospheric thermal radiation and sea ice growth. *J. Geophys. Res.,* **97** (C6), 9401–9410.

Verlinde, J., and Coauthors, 2007: The Mixed-Phase Arctic Cloud Experiment. *Bull. Amer. Meteor. Soc.,* **88,** 205–221.

Wyser, K., and Coauthors, 2008: An evaluation of Arctic cloud and radiation processes during the SHEBA year: Simulation results from eight Arctic regional climate models. *Climate Dyn.,* **30,** 203–222, doi:10.1007/s00382-007-0286-1.